DR XIAOHONG WANG (Orcid ID : 0000-0002-5065-2176)

DR HU MING-ZHE (Orcid ID : 0000-0003-0164-3326)

DR WEN LEI (Orcid ID : 0000-0003-1164-0233)

Article type : Article

A novel low-permittivity $LiAl_{0.98}(Zn_{0.5}Si_{0.5})_{0.02}O_2$-based microwave dielectric ceramics for LTCC application

Xue-Kai Lan[a,b], Jie Li[a,b], Fei Wang[a,b], Xiao-Chuan Wang[a,b], Wen-Zhong Lu[a,b], Ming-Zhe Hu[c], Wen Lei[a,b]*

[a] School of Optical and Electronic Information, Huazhong University of Science and Technology, Wuhan 430074, P. R. China

[b] Key Lab of Functional Materials for Electronic Information (B), Ministry of Education, Wuhan 430074, P. R. China

[c] School of Mechatronics Engineering, Guizhou Minzu University, Guiyang 550025, Guizhou, China

* Corresponding author. Tel.: +86 27 8755 6493; fax: +86 27 8754 3134.

E-mail address: wenlei@mail.hust.edu.cn (W. Lei)

This article has been accepted for publication and undergone full peer review but has not been through the copyediting, typesetting, pagination and proofreading process, which may lead to differences between this version and the Version of Record. Please cite this article as doi: 10.1111/ijac.13368

Abstract

Phase composition, morphology, and microwave dielectric properties of (1 - x) $LiAl_{0.98}(Zn_{0.5}Si_{0.5})_{0.02}O_2$ + x $CaTiO_3$ ($0.05 \leq x \leq 0.20$) materials synthesised via the solid state reaction method were investigated. All these densified materials were obtained at the sintering temperature of 1150 °C. All compositions showed a major $LiAlO_2$ phase that was accompanied by a minor $CaTiO_3$ phase. The ε_r value increases gradually from 10.88 to 11.60, whereas the $Q \times f$ value remarkably decreased from 33,251 GHz to 13,511 GHz. The τ_f value changes from -85 ppm/°C to 212 ppm/°C, thereby indicating that $CaTiO_3$ could effectively adjust this value. HBO_3-doping was used to further decrease the sintering temperature to 900 °C. The optimum value was obtained at 7 wt.% HBO_3 -doped with microwave dielectric properties of $\varepsilon_r = 9.39$, $Q \times f$ = 10, 224 GHz, and τ_f = -7.8 ppm/°C. This material also exhibited chemical compatibility with silver, making it a candidate for LTCC applications.

Introduction

Developing new microwave dielectric materials for the communication equipment such as resonators, filters and antennas, is necessary with the progress of wireless technology. [1-4] With the emergence of large scale integrated circuits, multi-chip component technology emerged, which is a high-density packaging technology for installing unpackaged integrated circuit (IC) chips on the same substrate, also known as advanced hybrid IC technology. Low temperature co-fired ceramics (LTCC) are considered as promising technology for the manufacture of advanced hybrid integrated circuits. Thus, materials for LTCC application have been extensively investigated in the past years. [5, 6] LTCC technology has the following important features [7-10]: a) reduces the sintering temperature of the materials below the melting temperature of metal electrode, like Ag (961 °C); b) materials do not react with the metal electrode; and c) materials must have a stable temperature coefficient of the resonant frequency (-10 ppm/°C $\leq \tau_f \leq$ 10 ppm/°C).

As an important microwave dielectric ceramic, $LiAlO_2$ has been investigated for its a potential. In the past year, we have conducted research on the substitution of Al^{3+} ions with equal molar amounts of Zn^{2+} and Si^{4+} ions to reform the microwave dielectric properties of the $LiAlO_2$ ceramic. [11] The result showed that the optimal property of the $LiAl_{1-x}(Zn_{0.5}Si_{0.5})_xO_2$ materials was obtained at x = 0.02. However, the constantly high sintering temperature (1300 °C) and large negative τ_f value (-122 ppm/°C) made this ceramic difficult to use for LTCC application. Usually, in the research area of LTCC technology, low melting temperatures of materials such as B_2O_3 [12], LiF [9, 13], LMZBS glass [14], $ZnO–B_2O_3$ glass [15], $CaO–B_2O_3–SiO_2$ glass [16], $BaO–B_2O_3–ZnO$ glass [17], and $Bi_2O_3–ZnO–B_2O_3–SiO_2$ glass [18] etc. were frequently used as sintering aids to lower the sintering temperature.

In this research, $CaTiO_3$ and HBO_3 were added to $LiAl_{0.98}(Zn_{0.5}Si_{0.5})_{0.02}O_2$ ceramic to solve the problems of high sintering temperature and large negative τ_f value in. The phase composition, morphologies, and microwave dielectric properties of (1-x) $LiAl_{0.98}(Zn_{0.5}Si_{0.5})_{0.02}O_2$ + x $CaTiO_3$ + y wt.% HBO_3 were then studied. Lastly, the chemical compatibility of this material with silver was investigated to meet the requirement for LTCC application.

Experimental procedure

$LiAl_{0.98}(Zn_{0.5}Si_{0.5})_{0.02}O_2$ ceramic was synthesized by using the conventional solid reaction process route. Stoichiometric Li_2CO_3, Al_2O_3, SiO_2, and ZnO reagents were blended with alcohol via ball milling for 5 h. Dried powder was then calcined in air at a furnace temperature of 900 °C for 3 h. The $CaTiO_3$ reagent with a ratio of (1-x) $LiAl_{0.98}(Zn_{0.5}Si_{0.5})_{0.02}O_2$ + x $CaTiO_3$ (x = 0.05 – 0.2) was added to the calcined $LiAl_{0.98}(Zn_{0.5}Si_{0.5})_{0.02}O_2$ powder and remilled in the same manner. The blended dried powder was then added into 10% PVA and follow sieved. And the granulated powder was pressed into pillars. Where after the pillars were sintered in air at 1150 °C for 6 h. For the samples containing HBO_3, the $0.9LiAl_{0.98}(Zn_{0.5}Si_{0.5})_{0.02}O_2$ + $0.1CaTiO_3$ + y wt.% HBO_3 (y = 1, 3, 5, 7) powder was also milled in alcohol for 5 h. And then drying in oven. Where after the dried powder was using the same forming procedures. Lastly, the HBO_3 -doped pillars were sintering in air at 900 °C for 3 h.

The crystal structures of (1 - x) $LiAl_{0.98}(Zn_{0.5}Si_{0.5})_{0.02}O_2$ + x $CaTiO_3$ and $0.9LiAl_{0.98}(Zn_{0.5}Si_{0.5})_{0.02}O_2$ + $0.1CaTiO_3$ + y wt.% HBO_3 ceramics were measured by using a Shimadzu XRD - 7000 X-ray diffractometer and the lattice parameters were obtained using the software GSAS. [19] The microstructure of thermal etching samples were obtained using a scanning electron microscope (SEM, Sirion 200, Netherlands). The ε_r and $Q\times f$ value of (1 -

x) $LiAl_{0.98}(Zn_{0.5}Si_{0.5})_{0.02}O_2$ + x $CaTiO_3$ (x = 0.05 – 0.2) and $0.9LiAl_{0.98}(Zn_{0.5}Si_{0.5})_{0.02}O_2$ + $0.1CaTiO_3$ + y wt.% HBO_3 ceramics were recorded by using the Hakki and Coleman method [20] and were detected by using a microwave network analyser (Agilent E8362B, Agilent Technologies, USA). Besides, the τ_f value of all the ceramics was obtained as follows [21]:

$$\tau_f = \frac{1}{f(T_0)} \frac{[f(T_1) - f(T_0)]}{T_1 - T_0}, \quad (1)$$

where $f(T_1)$ and $f(T_0)$ denote the resonant frequency measured at T_1 (80 °C) and T_0 (30 °C), respectively. Impedance spectroscopy analysis of the sample with coated Ag electrode was performed using an impedance analyzer in the frequency range of 100 Hz to 10 MHz. Moreover, all data were analyzed using in-house software.

Results and discussion

Fig. 1 shows the XRD patterns of (1 - x) $LiAl_{0.98}(Zn_{0.5}Si_{0.5})_{0.02}O_2$ + x $CaTiO_3$ (x = 0.05 – 0.20) ceramics sintered in air at 1150 °C for 6 h. This figure illustrated that these patterns exhibited only two phases of $LiAlO_2$ and $CaTiO_3$. On the basis of the profile intensity of the sample x = 0.05, Fig. 1(a) reveals that the $LiAlO_2$ phase is a major phase accompanied by a minor $CaTiO_3$ phase. The increase in the x value strengthened the main peak's intensity in the $CaTiO_3$ phase at approximately 33° of the 2θ axis, thereby indicating the increase in $CaTiO_3$ content. The Rietveld refinement method is used to obtain the lattice parameters of the series of materials. Fig. 2 shows the refinement results of the (1 - x) $LiAl_{0.98}(Zn_{0.5}Si_{0.5})_{0.02}O_2$ + x $CaTiO_3$ materials at x = 0.05 and x = 0.20 and Table 1 shows the lattice parameters of the $LiAl_{0.98}(Zn_{0.5}Si_{0.5})_{0.02}O_2$ and $CaTiO_3$ ceramics. As shown in Table 1, the lattice parameters of

$LiAl_{0.98}(Zn_{0.5}Si_{0.5})_{0.02}O_2$ and $CaTiO_3$ remain almost no changes, which also indicate there is no reaction between $LiAl_{0.98}(Zn_{0.5}Si_{0.5})_{0.02}O_2$ and $CaTiO_3$ material.

Fig. 3 shows the results of thermally etched morphologies and Energy Dispersive X-ray Detector (EDX) of $(1 - x)LiAl_{0.98}(Zn_{0.5}Si_{0.5})_{0.02}O_2 + xCaTiO_3$ ceramics sintered in air at 1150 °C for 6 h, that were observed via SEM. A dense microstructure with minimal porosity was detected in the samples (Fig. 3 (a) – 3 (d)). This result showed that the addition of $CaTiO_3$ could decrease the densification temperature of the $LiAl_{0.98}(Zn_{0.5}Si_{0.5})_{0.02}O_2$ ceramic, in which the optimal sintering temperature was 1300 °C. [11] In addition, all the samples in the SEM (Fig. 3 (a) – 3 (d)) presented the same grain with large and small parts. To further identify the phase compositions of different grains, EDX was used on the $(1-x)$ $LiAl_{0.98}(Zn_{0.5}Si_{0.5})_{0.02}O_2 + x\ CaTiO_3$ ($x = 0.1$) samples. The results (Fig. 3 (e) – 3 (h)) showed that the large grains were rich in Al element, thereby indicating that the samples were in the $LiAl_{0.98}(Zn_{0.5}Si_{0.5})_{0.02}O_2$ phase. By contrast, the small grains were rich in Ca and Ti elements, thereby indicating that these samples were in the $CaTiO_3$ phase. These results revealed that no reaction occurred between $LiAl_{0.98}(Zn_{0.5}Si_{0.5})_{0.02}O_2$ and $CaTiO_3$ ceramics.

Fig. 4 shows the microwave dielectric properties of $(1-x)$ $LiAl_{0.98}(Zn_{0.5}Si_{0.5})_{0.02}O_2 + x$ $CaTiO_3$ ceramics sintered in air at 1150 °C for 6 h. This figure illustrates that the ε_r value monotonously increased from 10.88 to 11.60 with the change in x from 0.05 to 0.20, whereas the $Q\times f$ value remarkably decreased from 33,251 GHz to 13,511 GHz. The τ_f value changed from -85 ppm/°C to 212 ppm/°C, thereby indicating that the near zero τ_f value can be achieved by adjusting the $CaTiO_3$ content. A near zero τ_f value could be obtained at $x = 0.10$

with the value of 9 ppm/°C. As shown in Fig. 3, all the compositions exhibit high densification. The ε_r, $Q \times f$ and τ_f values of a two-phase compact microwave dielectric composite ceramic generally obeys the following mixing rule [7, 22, 23]:

$$\ln \varepsilon_r = v_1 \ln \varepsilon_1 + v_2 \ln \varepsilon_2 ; \tag{2}$$

$$Q^{-1} = v_1 Q_1^{-1} + v_2 Q_2^{-1} ; \tag{3}$$

$$\tau_f = v_1 \tau_{f1} + v_2 \tau_{f2} ; \tag{4}$$

$$v_1 + v_2 = 1 . \tag{5}$$

where v_1 and v_2 represent the volume fractions of components, respectively. As we know, the $CaTiO_3$ microwave dielectric ceramic possesses high ε_r, low $Q\times f$ and large τ_f values. [24, 25] This feature of the $CaTiO_3$ material led to the increase in ε_r and τ_f values and a decrease in the $Q\times f$ value of (1-x) $LiAl_{0.98}(Zn_{0.5}Si_{0.5})_{0.02}O_2$ + x $CaTiO_3$ (x = 0.05 – 0.2) ceramics as the x value increased.

Fig. 5 exhibits the temperature dependency of the Arrhenius fit for the bulk conductivity (σ) of the (1-x) $LiAl_{0.98}(Zn_{0.5}Si_{0.5})_{0.02}O_2$ + x $CaTiO_3$ (x = 0.05 – 0.2) ceramics through impedance spectroscopy testing. With increased x from 0.05 to 0.2, the activation energy (E_a) calculated from the slope of the fitted line has a decrease tendency from 0.972 eV to 0.949 eV. Based on the approximation of the intrinsic band gap, $E_g \approx 2E_a$, [26-28] the conductivity is deduced to increase with increased x from 0.05 to 0.2. Thus, the sample at x = 0.05 has the highest quality factor for the (1-x) $LiAl_{0.98}(Zn_{0.5}Si_{0.5})_{0.02}O_2$ + x $CaTiO_3$ ceramics.

To further reduce the sintering temperature of (1-x) $LiAl_{0.98}(Zn_{0.5}Si_{0.5})_{0.02}O_2$ + x $CaTiO_3$ (x = 0.10) and meet the requirement for LTCC application, different HBO_3 contents were doped in the 0.9 $LiAl_{0.98}(Zn_{0.5}Si_{0.5})_{0.02}O_2$ + 0.1 $CaTiO_3$ material. Table 2 lists the microwave dielectric properties with different HBO_3 content added at a sintering temperature of 900 °C for 3 h. The ε_r value monotonously increased from 5.73 to 9.39, whereas the $Q\times f$ value increased from 2, 739 GHz to 10, 224 GHz. In addition, the τ_f value changed from 5.4 ppm/°C to -7.8 ppm/°C, thereby indicating that the optimum value was obtained at 7 wt.% HBO_3. Fig. 6 (a) shows the XRD pattern of the 7 wt.% HBO_3 doped 0.9 $LiAl_{0.98}(Zn_{0.5}Si_{0.5})_{0.02}O_2$ + 0.1 $CaTiO_3$ sample. Only two phases of $LiAlO_2$ and $CaTiO_3$ were revealed, and the HBO_3 content could be beyond the XRD limitation for detection. To verify the material chemical compatibility with Ag, the sample mixed with silver was sintered at 900 °C for 3 h. Fig. 7 shows the SEM and EDX of the 7 wt.% HBO_3 -doped $0.9LiAl_{0.98}(Zn_{0.5}Si_{0.5})_{0.02}O_2$ + $0.1CaTiO_3$ sample. Doping of 7 wt.% HBO_3 could obtain a dense sample at the lowered sintering temperature. Fig. 7 (a) illustrates two different large and small grains. The XRD pattern of Fig. 6 (b) shows that only $LiAlO_2$, $CaTiO_3$, and Ag phases exist. The EDX analysis in Fig. 7 (b - d) further demonstrated that no reaction was observed between the 7 wt.% HBO_3 -doped 0.9 $LiAl_{0.98}(Zn_{0.5}Si_{0.5})_{0.02}O_2$ + 0.1 $CaTiO_3$ sample and Ag.

Conclusion

In this work, a positive τ_f value of $CaTiO_3$ was added to compensate the τ_f value and solve the limitation of the large negative τ_f value of $LiAl_{0.98}(Zn_{0.5}Si_{0.5})_{0.02}O_2$ ceramic. Dense (1 - x) $LiAl_{0.98}(Zn_{0.5}Si_{0.5})_{0.02}O_2$ + x $CaTiO_3$ (x = 0.05 – 0.20) materials were synthesised via the solid-state reaction method at 1150 °C for 6 h. All the compositions showed two phases, and the EDX mapping manifested that no reactions occurred between $LiAl_{0.98}(Zn_{0.5}Si_{0.5})_{0.02}O_2$ and $CaTiO_3$. With the increase in $CaTiO_3$ content, a near zero sample was obtained at x = 0.10. HBO_3 was used to further decrease the sintering temperature. The use of 7 wt.% HBO_3 could effectively reduce the sintering temperature to 900 °C with suitable microwave dielectric properties for LTCC application. Lastly, the cofired test with silver proved that this material did not react with Ag.

Acknowledgements

This work was supported by the National Natural Science Foundation of China (NSFC-51572093, 51772107, 51567017 and 61771215), the Major Technological Innovation Projects in Hubei Province (2018AAA039), and the Research Projects Supported by the Equipment Development Department (1807WM0004). The authors are grateful to the Analytical and Testing Center, Huazhong University of Science and Technology, for SEM analyses.

Reference

[1] Chen HW, Su H, Zhang HW, Zhou TC, Zhang BW, Zhang JF, et al. Low-temperature sintering and microwave dielectric properties of $(Zn_{1-x}Co_x)_2SiO_4$ ceramics. Ceram. Int. 2014; 40(9); 14655-14659.

[2] Pang LX, Zhou D. Modification of $NdNbO_4$ microwave dielectric ceramic by Bi substitutions. J. Am. Ceram. Soc. 2019; 102(5); 2278-2282.

[3] Li L, Hong WB, Chen GY, Chen XM. High-performance $(1\text{-}x)(0.2B_2O_3–0.8SiO_2)–xTiO_2$ (x=0.025–0.1) glass matrix composites for microwave substrate applications. J. Alloy. Compd. 2019; 774; 706-709.

[4] Guo HH, Zhou D, Pang LX, Qi ZM. Microwave dielectric properties of low firing temperature stable scheelite structured (Ca, Bi)(Mo, V)O_4 solid solution ceramics for LTCC applications. J. Eur. Ceram. Soc. 2019; 39(7); 2365-2373.

[5] Pang LX, Zhou D. Modification of $NdNbO_4$ microwave dielectric ceramic by Bi substitutions. J. Am. Ceram. Soc. 2019; 102(5); 2278-2282.

[6] Zhou D. Pang LX, Wang D, Li C, Jin B, Reaney IM. High permittivity and low loss microwave dielectrics suitable for 5G resonators and low temperature co-fired ceramic architecture. J. Mater. Chem. C 2017; 5(38); 10094-10098.

[7] Zhang J, Zuo R, Song J, Xu Y, Shi M. Low-loss and low-temperature firable $Li_2Mg_3SnO_6$-$Ba_3(VO_4)_2$ microwave dielectric ceramics for LTCC applications. Ceram. Int. 2018; 44(2); 2606-2610.

[8] Wang K, Zhou H, Liu X, Sun W, X. Chen, Ruan H. A lithium aluminium borate

composite microwave dielectric ceramic with low permittivity, near-zero shrinkage, and low sintering temperature. J. Eur. Ceram. Soc. 2019; 39(4); 1122-1126.

[9] Lai Y, Su H, Wang G, Tang X, Huang X, Liang X, et al. Low- temperature sintering of microwave ceramics with high Qf values through LiF addition. J. Am. Ceram. Soc. 2019; 102(4); 1893-1903.

[10] Zhang Z, Fang L, Xiang H, Xu M, Tang Y, Jantunen H, et al. Structural, infrared reflectivity spectra and microwave dielectric properties of the $Li_7Ti_3O_9F$ ceramic. Ceram. Int. 2019; 45(8); 10163-10169.

[11] Lan XK, Li J, Zou ZY, Fan GF, Lu WZ, Lei W. Lattice structure analysis and optimised microwave dielectric properties of $LiAl_{1-x}(Zn_{0.5}Si_{0.5})_xO_2$ solid solutions. J. Eur. Ceram. Soc. 2019; 39(7); 2360-2364.

[12] Li C, Xiang H, Yin C, Tang Y, Li Y, Fang L. Ultra-Low Loss Microwave Dielectric Ceramic $Li_2Mg_2TiO_5$ and Low-Temperature Firing Via B_2O_3 Addition. J. Electron. Mater. 2018; 47(11); 6383-6389.

[13] Pan H, Liu M, Li M, Ling F, Wu H. Low temperature sintering and microwave dielectric properties of $Li_6Mg_7Ti_3O_{16}$ ceramics with LiF additive for LTCC applications. J. Mater. Sci.-Mater. El. 2018; 29(2); 999-1003.

[14] Qin T, Zhong C, Yang H, Qin Y, Zhang S. Investigation on glass-forming ability, Flexural strength and microwave dielectric properties of Al_2O_3-doped LMZBS glasses. Ceram. Int. 2019; 45(8); 10899-10906.

[15] Lan XK, Zou ZY, Lu WZ, Zhu JH, Lei W. Phase transition and low-temperature

sintering of $Zn(Mn_{1-x}Al_x)_2O_4$ ceramics for LTCC applications. Ceram. Int. 2016; 42(15); 17731-17735.

[16] Xia Y, Hu Y, Ren L, Luo X, Gong W, Zhou H. Manufacturing a high performance film of CaO-B_2O_3-SiO_2 glass-ceramic powder with surface modification for LTCC application. J. Eur. Ceram. Soc. 2018; 38(1); 253-261.

[17] Shu G, Zhang Q, Yang F, Meng F, Lin H. Low temperature sintering and microwave dielectric properties of Li_2 $ZnTi_3O_8$–TiO_2 ceramics doped with BaO–B_2O_3–ZnO glass. J. Mater. Sci.-Mater. El. 2018; 29(19); 17008-17015.

[18] Qi S, Cheng H, Yang K, Song B, Sun S, Zhang Y. Effects of Bi_2O_3–ZnO–B_2O_3–SiO_2 glass addition on the sintering and microwave dielectric properties of $ZnZrNb_2O_8$ ceramics for LTCC applications. J. Mater. Sci.-Mater. El. 2019; 30(7); 6411-6418.

[19] Toby BH. Expgui, A Graphical User Interface for GSAS. J Appl Crystallogr. 2001; 34(2); 210-213.

[20] Hakki B, Coleman P. A dielectric resonator method of measuring inductive capacities in the millimeter range. IEEE Trans. Microw. Theory Tech. 1960; 8(4); 402-410.

[21] Jing X, Su H, Jing Y, Li Y, Tang X. Structure and microwave dielectric behaviour of low-temperature-fired $Li_2Zn_{1-x}Co_xTi_3O_8$ (x=0–0.07) ceramics for low temperature co-fired ceramic applications. J. Mater. Sci.-Mater. El. 2019; 30(8); 7711-7716.

[22] Ren J, Bi K, Fu X, Peng Z. Novel $Al_2Mo_3O_{12}$-based temperature-stable microwave dielectric ceramics for LTCC applications. J. Mater. Chem. C 2018; 6(42); 11465-11470.

[23] Weng Z, Song C, Xiong Z, Xue H, Sun W, Zhang Y, et al. Microstructure and broadband

dielectric properties of Zn_2SiO_4 ceramics with nano-sized TiO_2 addition. Ceram. Int. 2019; 45(10); 13251-13256.

[24] Yuan S, Gan L, Ning F, An S, Jiang J, Zhang T. High-$Q\times f$ 0.95$MgTiO_3$–0.05$CaTiO_3$ microwave dielectric ceramics with the addition of LiF sintered at medium temperatures. Ceram. Int. 2018; 44(16); 20566-20569.

[25] Kai C, Li C, Xiang H, Tang Y, Sun Y, Fang L. Phase formation and microwave dielectric properties of $BiMVO_5$ (M = Ca, Mg) ceramics potential for low temperature co-fired ceramics application. J. Am. Ceram. Soc. 2019; 102(1); 362-371.

[26] Li M, Pietrowski MJ, De Souza RA, Zhang H, Reaney IM, Cook SN, et al. A family of oxide ion conductors based on the ferroelectric perovskite $Na_{0.5}Bi_{0.5}TiO_3$. Nat. mater. 2014; 13(1); 31-35.

[27] Zang J, Li M, Sinclair DC, Fromling T, Jo W, Rodel J. Impedance Spectroscopy of $(Bi_{1/2}Na_{1/2})TiO_3$–$BaTiO_3$ Based High-Temperature Dielectrics. J. Am. Ceram. Soc. 2014; 97(9); 2825-2831.

[28] Rawal R, Feteira A, Flores AA, Hyatt NC, West AR, Sinclair DC, et al. Dielectric Properties of the "Twinned" 8H-Hexagonal Perovskite $Ba_8Nb_4Ti_3O_{24}$. J. Am. Ceram. Soc. 2006; 89(1); 336-339.

Table 1 Lattice parameters of (1 - x) $LiAl_{0.98}(Zn_{0.5}Si_{0.5})_{0.02}O_2$ + x $CaTiO_3$ ceramics, the subscript 1 $LiAl_{0.98}(Zn_{0.5}Si_{0.5})_{0.02}O_2$ represent and subscript 2 represent $CaTiO_3$.

Sample	**0.05**	**0.10**	**0.15**	**0.20**
a_1(Å)	5.169	5.167	5.168	5.167
c_1(Å)	6.294	6.295	6.294	6.296
a_2(Å)	5.371	5.371	5.372	5.372
b_2(Å)	7.645	7.644	7.645	7.644
c_2(Å)	5.439	5.438	5.439	5.437

Table 2 Microwave dielectric properties of 0.9 $LiAl_{0.98}(Zn_{0.5}Si_{0.5})_{0.02}O_2$ + 0.1 $CaTiO_3$ + y wt% HBO_3 ceramics sintered at 900 °C for 3 h.

y value	ε_r	$Q \times f$ (GHz)	τ_f (ppm/°C)
1	5.73	2739	5.4
3	7.04	3331	-1.6
5	7.99	6139	-4.2
7	9.39	10224	-7.8

Figure captions:

Fig. 1 XRD patterns of the (1 - x) $LiAl_{0.98}(Zn_{0.5}Si_{0.5})_{0.02}O_2$ + x $CaTiO_3$ ceramics sintered at 1150 °C in air for 6 h: (a) x=0.05; (b) x=0.10; (c) x=0.15; (d) x=0.20.

Fig. 2 Rietveld refinement of (a) (1 - x) $LiAl_{0.98}(Zn_{0.5}Si_{0.5})_{0.02}O_2$ + x $CaTiO_3$ (x = 0.05) and (b) (1 - x) $LiAl_{0.98}(Zn_{0.5}Si_{0.5})_{0.02}O_2$ + x $CaTiO_3$ (x = 0.20) ceramic.

Fig. 3 SEM micrograph and EDX of the (1 - x) $LiAl_{0.98}(Zn_{0.5}Si_{0.5})_{0.02}O_2$ + x $CaTiO_3$ ceramics sintered at 1150 °C for 6 h in air atmosphere: (a) x = 0.05; (b) x = 0.1; (c) x = 0.15; (d) x = 0.2; (e) x = 0.1; (f) Al content; (g) Ca content; (h) Ti content.

Fig. 4 The microwave dielectric properties of the (1 - x) $LiAl_{0.98}(Zn_{0.5}Si_{0.5})_{0.02}O_2$ + x $CaTiO_3$ (x = 0.05 –0.20) ceramics as a function of x value.

Fig. 5 Arrhenius fitting plot from the temperature dependence of the bulk conductivity for (1 - x) $LiAl_{0.98}(Zn_{0.5}Si_{0.5})_{0.02}O_2$ + x $CaTiO_3$ ceramics.

Fig. 6 (a) XRD pattern of 0.9 $LiAl_{0.98}(Zn_{0.5}Si_{0.5})_{0.02}O_2$ + 0.1 $CaTiO_3$ + 7 wt% HBO_3; (b) XRD pattern of Ag co-fired sample.

Fig. 7 (a) SEM of 0.9 $LiAl_{0.98}(Zn_{0.5}Si_{0.5})_{0.02}O_2$ + 0.1 $CaTiO_3$ + 7 wt.% HBO_3; (b) Ag content; (c) Al content; (d) Ti content.

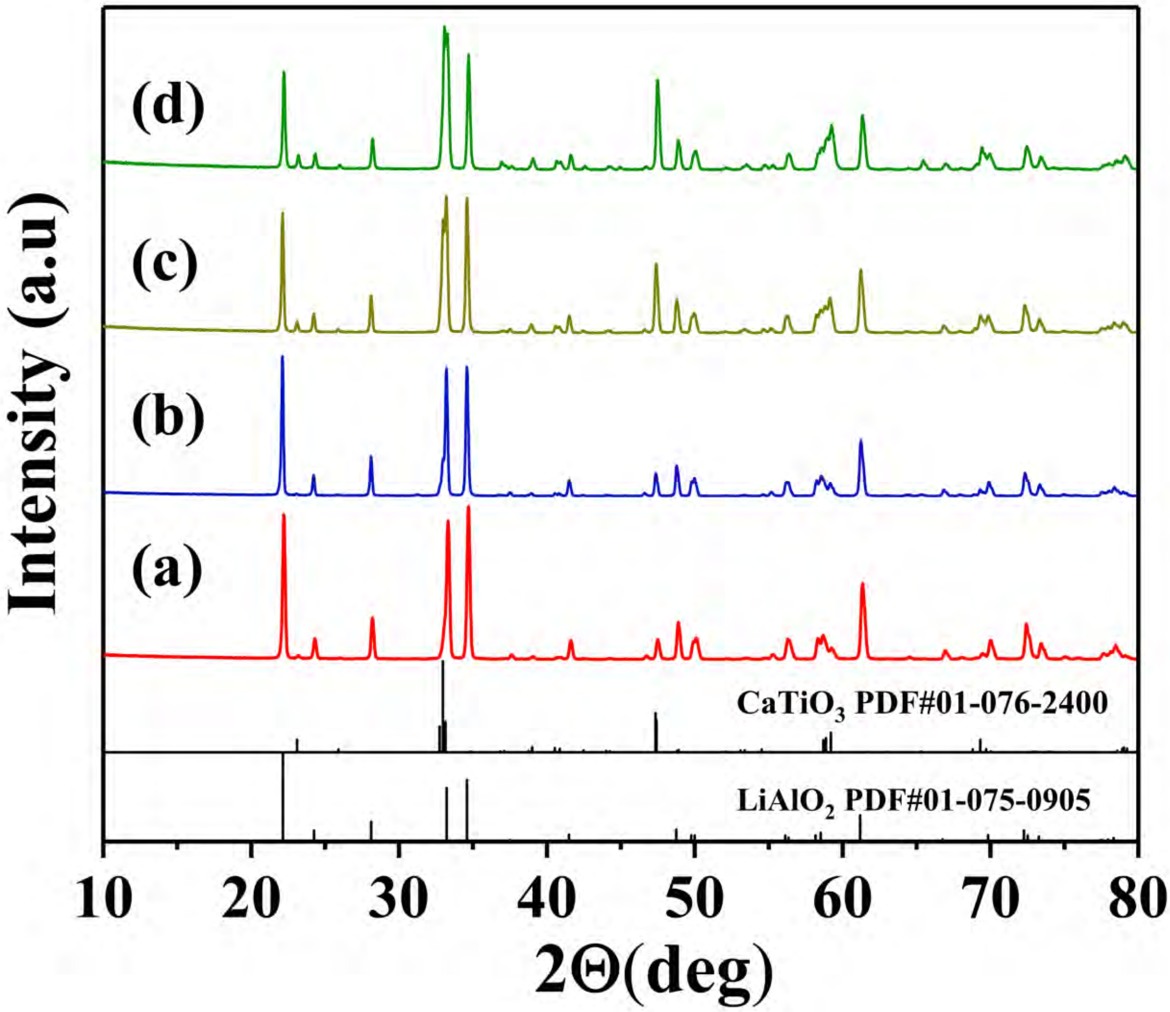

(d)
(c)
(b)
(a)
Intensity (a.u)
$CaTiO_3$ PDF#01-076-2400
$LiAlO_2$ PDF#01-075-0905
10 20 30 40 50 60 70 80
2Θ(deg)

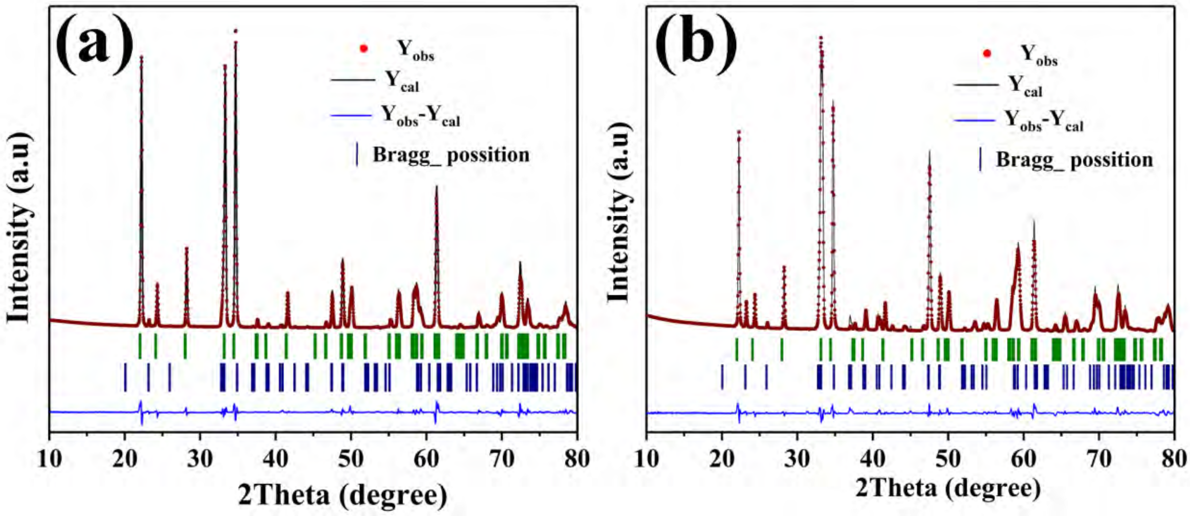

(a)
Y_{obs}
Y_{cal}
Y_{obs}-Y_{cal}
Bragg_ possition
Intensity (a.u)
2Theta (degree)
(b)
Y_{obs}
Y_{cal}
Y_{obs}-Y_{cal}
Bragg_ possition
Intensity (a.u)
2Theta (degree)

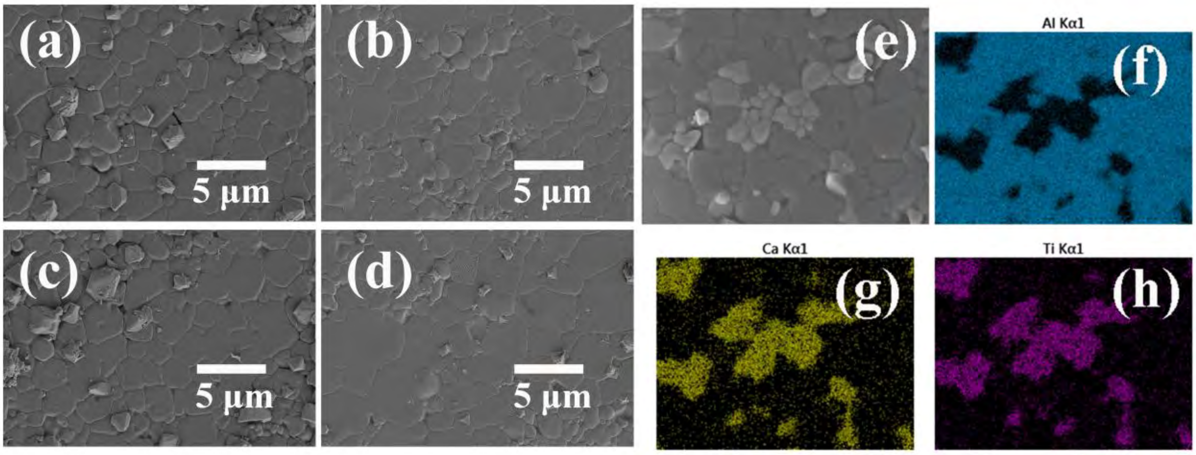
(a)
5 µm
(b)
5 µm
(c)
5 µm
(d)
5 µm
(e)
Al Kα1
(f)
Ca Kα1
(g)
Ti Kα1
(h)

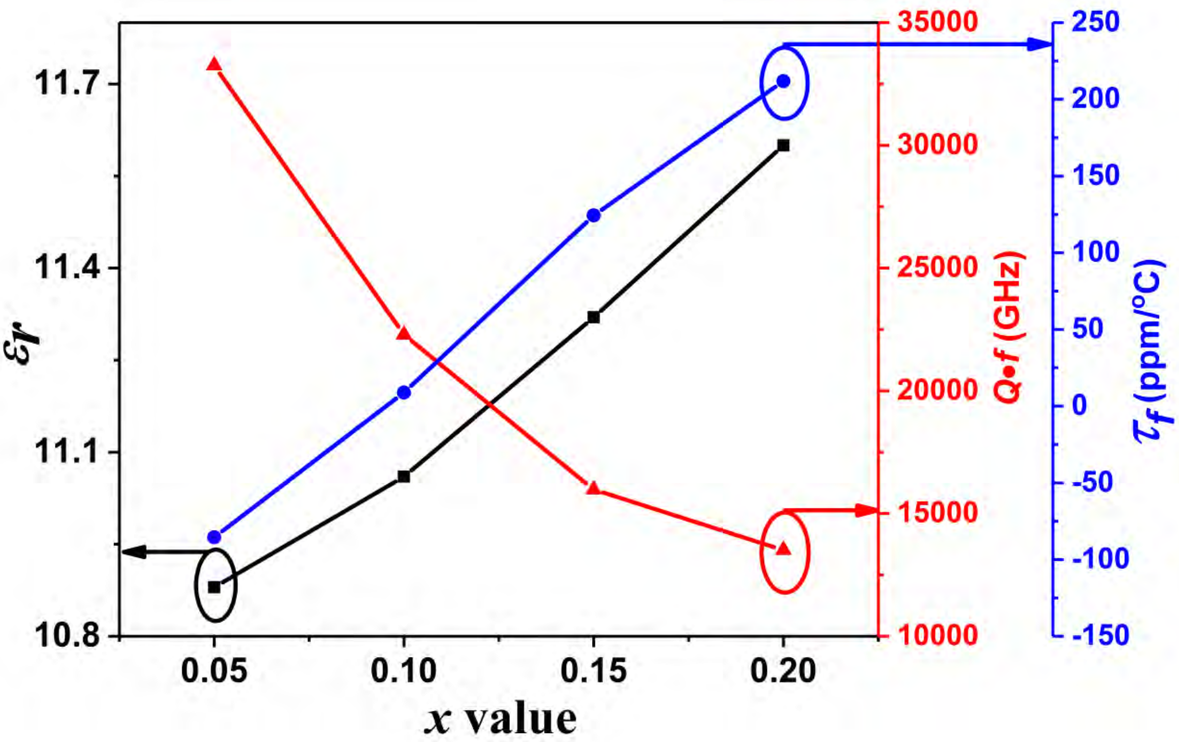
11.7
11.4
11.1
10.8
ε_r
35000
30000
25000
20000
15000
10000
Q•f (GHz)
250
200
150
100
50
0
-50
-100
-150
τ_f (ppm/°C)
0.05
0.10
0.15
0.20
x value

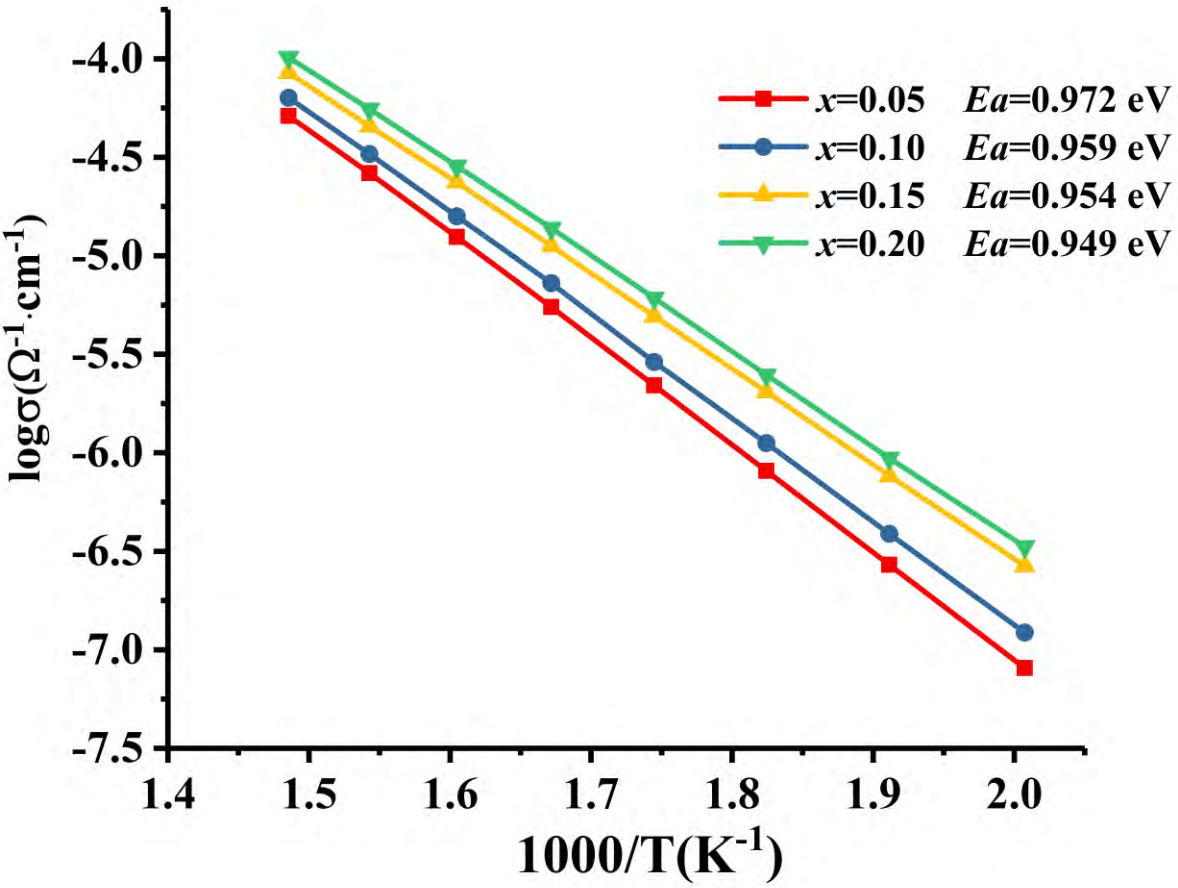

x=0.05 Ea=0.972 eV
x=0.10 Ea=0.959 eV
x=0.15 Ea=0.954 eV
x=0.20 Ea=0.949 eV
logσ(Ω-1·cm-1)
1000/T(K-1)
-4.0
-4.5
-5.0
-5.5
-6.0
-6.5
-7.0
-7.5
1.4
1.5
1.6
1.7
1.8
1.9
2.0

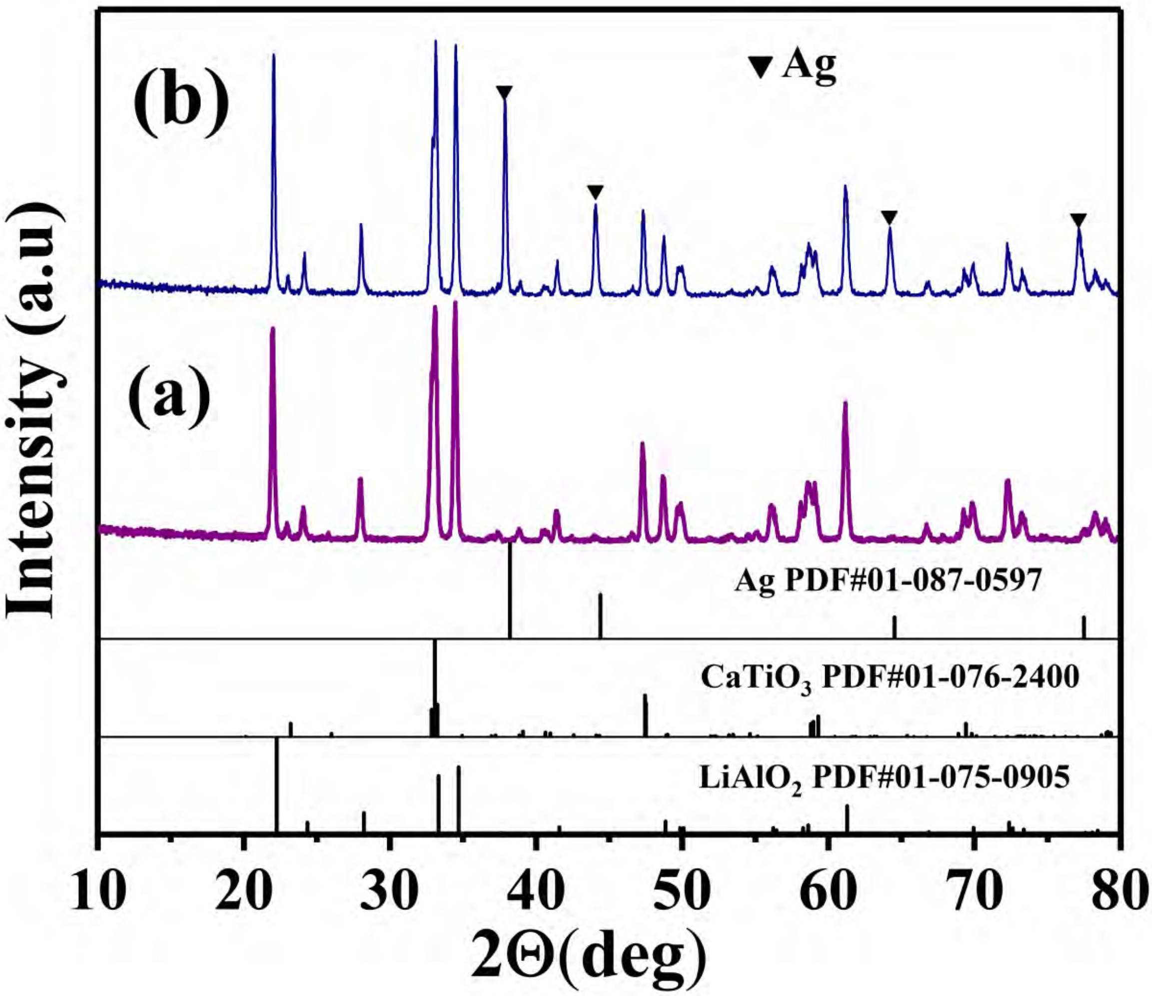

(b)
▼ Ag
(a)
Intensity (a.u)
Ag PDF#01-087-0597
CaTiO3 PDF#01-076-2400
LiAlO2 PDF#01-075-0905
10
20
30
40
50
60
70
80
2Θ(deg)

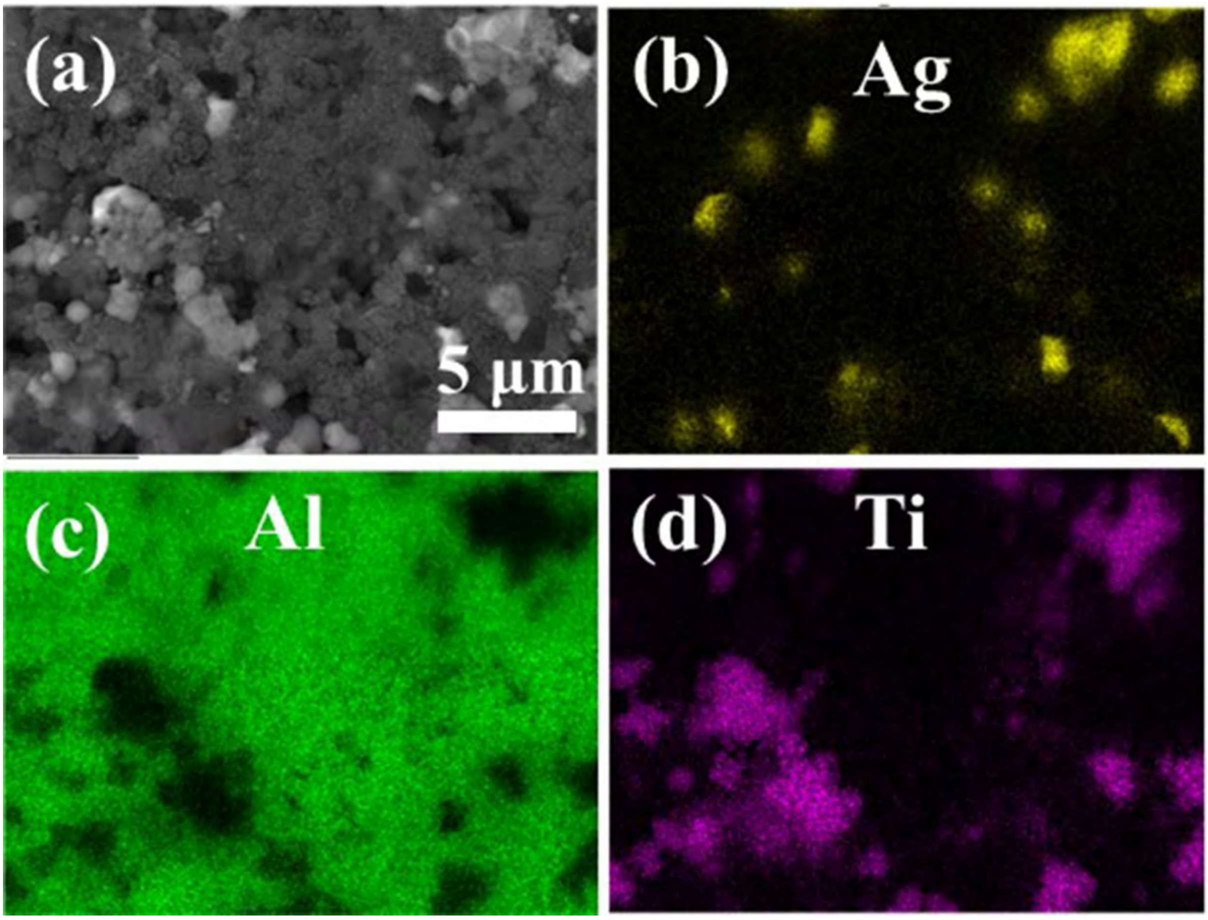
(a)
5 µm
(b) Ag
(c) Al
(d) Ti